

Gamma-ray bursts as dark energy-matter probes in the context of the generalized Chaplygin gas model.

O. Bertolami^{*} and P.T. Silva[†]

Instituto Superior Técnico, Departamento de Física, Avenida Rovisco Pais, 1, 1049-001, Lisboa, Portugal

Accepted . Received ;

ABSTRACT

In this paper we consider the use of Gamma Ray Bursts (GRBs) as distance markers to study the unification of dark energy and dark matter in the context of the so-called Generalized Chaplygin Gas (GCG) model. We consider that the GRB luminosity may be estimated from its variability, time-lag, and also use the so-called Ghirlanda relation. We evaluate the improvements one may expect once more GRBs and their redshift become available. We show that although GRBs allow for extending the Hubble diagram to higher redshifts, its use as a dark energy probe is limited when compared to SNe Ia. We find that the information from GRBs can provide some bounds on the amount of dark matter and dark energy independently of the equation of state. This is particularly evident for XCDM-type models, which are, for low-redshifts ($z \leq 2$), degenerate with the GCG.

Key words: Cosmology: observations - cosmological parameters - dark matter - distance scale - gamma-rays: bursts - methods: miscellaneous

1 INTRODUCTION

The GCG model (Kamenshchik, Moschella & Pasquier 2001; Bento, Bertolami & Sen 2002b) is an interesting alternative to more conventional approaches for explaining the observed accelerated expansion of the Universe such as a cosmological constant (see e.g. Bento & Bertolami 1999; Bento, Bertolami & Silva 2001) or quintessence (Ratra & Peebles 1988a, 1988b; Wetterich 1988; Caldwell, Dave & Steinhardt 1998; Ferreira & Joyce 1998; Zlatev, Wang & Steinhardt 1999; Binétruy 1999; Kim 1999; Uzan 1999; Chiba 1999; Amendola 1999; Albrecht & Skordis 2000; Fujii 2000; Bertolami & Martins 2000; Sen, Sen & Sethi 2001; Sen & Sen 2001; Bento, Bertolami & Santos 2002). It is worth remarking that quintessence is related to the idea that the cosmological term could evolve (Bronstein 1933; Bertolami 1986a; Bertolami 1986b; Ozer & Taha 1987) and with attempts to solve the cosmological constant problem.

In the GCG approach one considers an exotic equation of state to describe the behaviour of the background fluid:

$$p_{ch} = -\frac{A}{\rho_{ch}^\alpha}, \quad (1)$$

where A and α are positive constants. The case $\alpha = 1$ corresponds to the Chaplygin gas. In most phenomenological studies the range

$0 < \alpha \leq 1$ is considered. Within the framework of Friedmann-Robertson-Walker cosmology, this equation of state leads, after being inserted into the relativistic energy conservation equation, to an evolution of the energy density as (Bento et al. 2002b)

$$\rho_{ch} = \left[A + \frac{B}{a^{3(1+\alpha)}} \right]^{\frac{1}{1+\alpha}}, \quad (2)$$

where a is the scale-factor of the Universe and B a positive integration constant. From this result, one can understand a striking property of the GCG: at early times the energy density behaves as matter while at late times it behaves like a cosmological constant. This behaviour suggests the interpretation of the GCG model as an entangled mixture of dark matter and dark energy.

This model has several attractive features. From a theoretical point of view, the pure Chaplygin model ($\alpha = 1$) equation of state can be obtained from the Nambu-Goto action for d -branes moving in a $(d + 2)$ -dimensional spacetime in the light cone parameterization (Bordemann & Hoppe 1993). It is also the only fluid which admits a supersymmetric generalization (Jackiw & Polychronakos 2000), and also appeared in the study of the stabilization of branes in bulks with a black hole geometry (Kamenshchik, Moschella & Pasquier 2000). The Chaplygin gas may be viewed as a quintessence field with a suitable potential (Kamenshchik et al. 2001), or as an effect arising from the embedding of a $(3 + 1)$ -dimensional brane in a $(4 + 1)$ -dimensional bulk (Bilic, Tupper & Viollier 2002). The generalized Chaplygin gas also has a connection with brane theories (Bento et al. 2002b). The model can be yet viewed as the sim-

^{*} E-mail: orfeu@cosmos.ist.utl.pt

[†] E-mail:paptms@ist.utl.pt

2 O. Bertolami & P.T. Silva

plest model within the family of tachyon cosmological models (Frolov, Kofman & Starobinsky 2002).

The GCG model has also been successfully confronted with different classes of phenomenological tests: high precision Cosmic Microwave Background Radiation data (Bento, Bertolami & Sen 2003a; Bento, Bertolami & Sen 2003b; Bento, Bertolami & Sen 2003c; Caturan & Finelli 2003; Amendola et al. 2003), supernova data (Fabris, Gonçalves & Souza 2002a; Dev, Alcaniz & Jain 2003; Gorini, Kamenshchik & Moschella 2003; Makler, Oliveira & Waga 2003; Alcaniz, Jain & Dev 2003; Bertolami et al. 2004; Bento et al. 2005), and gravitational lensing (Silva & Bertolami 2003; Dev, Jain & Alcaniz 2004). More recently, it has been shown using the latest supernova data (Tonry et al. 2003; Barris et al. 2004; Riess et al. 2004), that the GCG model is degenerate with a dark energy model with a phantom-like equation of state (Bertolami et al. 2004; Bento et al. 2005). Furthermore, it can be shown that this does not involve any violation of the dominant energy condition and hence does not lead to the big rip singularity in future (Bertolami et al. 2004). It is a feature of GCG model, that it can mimic a phantom-like equation of state, but without any kind of pathologies as asymptotically the GCG approaches to a well-behaved de-Sitter universe. Structure formation in the context of the Chaplygin gas and the GCG was originally examined in Bento et al. (2002b), Bilic et al. (2002) and Fabris, Gonçalves & Souza (2002b). The results of the various phenomenological tests on the GCG model are summarized in Bertolami (2004) and Bertolami (2005).

Subsequently, concerns about such an unified model were raised in the context of structure formation. Indeed, it has been pointed out that one should expect unphysical oscillations or even an exponential blow-up in the matter power spectrum (Sandvik et al. 2003), given the behaviour of the sound velocity through the GCG. Although, at early times, the GCG behaves like dark matter and its sound velocity is vanishingly small, at later times the GCG starts behaving like dark energy with a substantial negative pressure yielding a large sound velocity which, in turn, can produce oscillations or blow-up in the power spectrum. This is a common feature of any unified approach when the dark matter and the dark energy components of the fluid are not clearly identified. These components are, of course, interacting, as they make part of the same fluid. It can be shown however that the GCG is a unique mixture of interacting dark matter and a cosmological constant-like dark energy, once one excludes the possibility of phantom-type dark energy (Bento, Bertolami & Sen 2004). It can be shown that due to the interaction between the components, there is a flow of energy from dark matter to dark energy. This energy transfer is not significant until the recent past, resulting in a negligible contribution at the time of gravitational collapse ($z_c \simeq 10$). Subsequently, at about $z \simeq 2$, the interaction starts to grow yielding a large energy transfer from dark matter to dark energy, which leads to the dominance of the latter at present. Actually, it is shown that the epoch of dark energy dominance occurs when dark matter perturbations start deviating from its linear behaviour and that the Newtonian equations for small scale perturbations for dark matter do not involve any mode-dependent term. Thus, neither oscillations nor blow-up in the power spectrum do develop.

In this paper we study yet another cosmological test and its possible use to study the GCG. Schaefer (2002) suggested that Gamma Ray Bursts (GRBs) may be used to extend the Hubble diagram to redshifts as high as $z \sim 5$. For ‘ordinary’ dark energy, such

high redshifts are not very interesting since at those epochs the Universe is dominated by dark matter, and thus it is less sensitive to the nature of dark energy.

For the GCG however, the GRB test might be relevant since it unifies dark energy and dark matter into one single fluid. Therefore, within the framework of the GCG model, the dark matter domination period actually depends of the nature of the dark energy component that kicks in at later times, and one can expect that the study of the matter dominated era will bring some insight on some properties of GCG models.

This paper is organized as follows; in section 2 we explain our method of using the time-lag/luminosity and variability/luminosity correlations to constrain cosmological models. In section 3 we present and comment the results obtain from this method. In section 4 we consider a more precise correlation found by Ghirlanda, Ghisellini & Lazzati (2004a), and study its consequences. In section 5 we consider whether it is possible to use the extended redshift range of GRBs to break the degeneracy between the GCG and the XCDM (cold dark matter plus a dark energy component with a constant equation of state). Finally in section 6 we discuss our results and present our conclusions.

2 METHOD.

2.1 Overview.

The starting point of our study is the proposed correlation between time lags in GRBs spectra and the isotropic equivalent luminosity (Norris, Marani & Bonnell 2000), and the correlation between GRB variability and isotropic equivalent luminosity (Reichart et al. 2001). The time lag, denoted by τ_{lag} , measures the time offset between high and low energy GRB photons that arrive on Earth. The variability, V , is easily defined in qualitative terms as a measurement of the ‘spikiness’ or complexity of the GRB light curve. The isotropic equivalent luminosity is the inferred luminosity of a GRB if all its energy is radiated isotropically. That is, if P is the peak flux of a burst in units of photons $\text{cm}^{-2}\text{s}^{-1}$ between observer frame energies E_l and E_u , the isotropic equivalent peak photon luminosity of the burst in erg s^{-1} between source frame energies 300 keV and 2000 keV is given by

$$L_{iso} = 4\pi r^2(z) P \frac{\int_{300}^{2000} EN[E/(1+z)]dE}{\int_{E_l}^{E_u} N(E)dE} \quad (3)$$

where $N(E)$ is the observer frame spectral shape, usually parameterized by a Band function (Band et al. 1993), and $r(z)$ is the comoving distance to a burst at redshift z .

The possible use of this relation to expand the Hubble diagram to higher redshifts was first discussed in Schaefer (2002). One limitation of the employed method is the cosmological distances of GRBs, which affect the ability of performing a proper calibration of their distance independently of the background cosmology. One has to either fix a cosmological model and find a calibration that depends on the assumed cosmological model, or fit the data to both calibration and cosmological parameters. This degrades precision since there are more free parameters for the same number of data points.

One way around this was proposed by Takahashi et al. (2003). Let us assume that one measures the luminosity distance up to $z = z_{max}$, with say $z_{max} = 1.5$. This is, for instance, very likely to be

possible with the SNAP¹ mission. This means that one would have an estimate of the absolute isotropic luminosity that is independent of the calibration and of the cosmological model. One may then use these estimates to calibrate the (τ_{lag}, L_{iso}) and (V, L_{iso}) relations without assuming a background cosmological model.

The major strength of GRBs as cosmological probes is that they can be found at very high redshifts (Lamb & Reichart 2000). One may then use high-redshift GRBs data to probe the cosmology. This is performed by using the (τ_{lag}, L_{iso}) and (V, L_{iso}) relations to estimate the luminosity distance at higher redshifts. A possible method would consist in using GRBs with $z < 1.5$ together with the luminosity distance estimates from supernovae to calibrate the luminosity estimator, and then use this calibration to find the luminosity distance of GRBs with $z > 1.5$. It should be noted that this method aims to study the luminosity distance at the range $1.5 < z < 5$. Later it will be shown that adding information obtained in the range $z < 1.5$ is actually crucial to the study of dark energy models.

With this information, one may estimate the luminosity distance at high redshifts, and place constraints on the cosmological parameters via a standard χ^2 minimization procedure.

The aim of this paper is to use this method to constrain the GCG unification model of dark energy and dark matter. Even though it is shown that the optimum redshift range for studying dark energy is around $z < 2$ (Huterer & Turner 2000), as already remarked, since the GCG also describes dark matter, a higher redshift range might be relevant for a better understanding of the model.

Our study will be performed in three steps. First we build a realistic mock distribution of GRBs in redshift and isotropic luminosity space (section 2.2). Second, we test the calibration procedure to find what improvements might be achieved in the future. To do this we shall consider a fiducial set of calibration parameters to generate a mock set of time lags and variabilities for each GRB. We shall then perform a χ^2 fit to this mock data to study the calibration precision. The last step consists in employing this method to probe GCG models. This will be done in a fashion similar to what was already performed with SNe Ia (Goliath et al. 2001; Weller & Albrecht 2002; Di Pietro & Claeskens 2003; Silva & Bertolami 2003). A fiducial cosmological model is assumed, and regions of constant χ^2 will be plotted around the fiducial set of parameters.

2.2 Generating a GRB mock population.

We describe here the process of population generation. We simulate several data sets, which differ only in size. We consider three sample sizes. The first sample is composed of 90 GRBs, and is consistent with the expected number of GRBs with measured redshift $z > 1.5$ that is what the SWIFT satellite is expected to detect in its three year mission (Schaefer 2002). The second and third samples are larger and contain 500 and 1000 GRBs, respectively, and serve as best case scenarios to test whether further data might improve the results.

The GRBs in each sample are distributed in redshift and luminosity according to the GRB rate history and luminosity function based on the model of the star formation 2 from Porciani & Madau (2002). The energy spectrum of the GRB is assumed to be a single power law with index -2.5. The flux limit

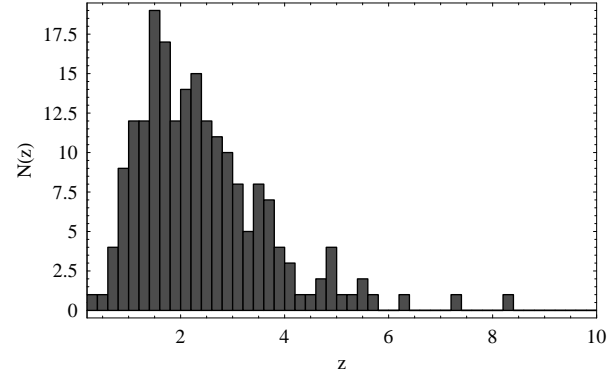


Figure 1. The redshift distribution of a GRB sample population.

Parameter	Value
B_v	$10^{55.32}$
β_v	1.57
σ_v	0.20
B_τ	$10^{50.03}$
β_τ	-1.27
σ_τ	0.35

Table 1. Values used in the calibration test.

of the SWIFT satellite, $f > 0.04$ photons $\text{cm}^{-2}\text{s}^{-1}$ is applied to check whether the GRB can be detected. The observed magnitude is calculated assuming a flat ΛCDM cosmological model, with $\Omega_\Lambda = 0.7$ and $H_0 = 70 \text{ km s}^{-1} \text{ Mpc}^{-1}$.

We show an example of a generated sample in Figure 1.

2.3 Calibration procedure.

Reichart et al. (2001) proposed a relation between the variability and isotropic equivalent luminosity of a GRB such that

$$L_{iso} = B_v V^{\beta_v}, \quad (4)$$

while Norris et al. (2000) proposed a similar relation between τ_{lag} and L_{iso} ,

$$L_{iso} = B_\tau \tau_{lag}^{\beta_\tau}. \quad (5)$$

As already mentioned, the first step in testing the calibration procedure consists in establishing a fiducial model. Schaefer (2002) used the nine GRBs with available redshifts at the time to calibrate these relations, yielding:

$$\beta_v = 1.57; \quad B_v = 10^{50.03}; \quad (6)$$

$$\beta_\tau = -1.27; \quad B_\tau = 10^{55.32}. \quad (7)$$

We shall assume these values as our fiducial model, i.e. we suppose that the calibration relations are faithful, and that they are described by this set of parameters. For each GRB of the mock luminosity distribution, generated as we explained above, we compute the corresponding time lag, τ_{lag} , and variability, V , through

$$\log \tau_{lag} = \log B_\tau + \frac{1}{\beta_\tau} \log L + \text{Random}(\sigma_\tau), \quad (8)$$

$$\log V = \log B_v + \frac{1}{\beta_v} \log L + \text{Random}(\sigma_v), \quad (9)$$

where the $\text{Random}(\sigma)$ term is a pseudo random number drawn

¹ www.snap.gov

N_{GRB} used in calibration	σ_{β_τ}	σ_{β_V}	σ_μ (mag.)
40	0.053	0.021	0.68
100	0.033	0.014	0.66
200	0.023	0.010	0.66

Table 2. Results from calibration test. The last column refers to the uncertainty of the distance modulus determination using our method.

from a normal distribution with zero mean value and variance σ . That is, we assume that τ_{lag} and V have lognormal error distributions, with variance σ_τ and σ_v , respectively.

The values we use for σ_v and σ_τ are based on Schaefer (2002) and are essentially dominated by an intrinsic (statistical) error. The used fiducial values are shown in Table 1.

In the real situation, we would assume that the luminosity distance at redshifts smaller than $z = 1.5$ has been measured independently by SNe Ia experiments, such as SNAP. Knowledge of the peak flux observed on Earth, and the spectral shape $N(E)$ allow obtaining the corresponding equivalent isotropic luminosity from Eq. (3).

We do not consider errors in this estimate of L_{iso} , but it should be noted that it is expected that the luminosity distance uncertainty will be around $\sigma_{\log d_L} \sim 0.01$ for future experiments such as SNAP (Goliath et al. 2001; Weller & Albrecht 2002). This translates into $\sigma_{\log L} \sim 0.02$, a much smaller error than the intrinsic scatter of GRBs. Thus, this source of uncertainty should not influence our conclusions.

Notice that we have used low-redshift GRBs from the generated sample to calibrate the relations Eqs. (4) and (5) through a standard χ^2 fitting procedure. That is, our procedure consisted in:

- Generating a GRB sample.
- For each GRB in the sample, assigning a time lag and variability via Eqs. (8) and (9).
- Fitting the calibration relations Eqs. (4) and (5) for the low- z GRBs from the mock sample.
- Repeating the steps for different size samples, and study the precision of the attained fits.

Our results are shown in Table 2. The smaller sample size corresponds to what is expected to be found by the SWIFT satellite in its three year campaign, the second sample size corresponds to the number of low- z GRBs that should be found if there were about 500 GRBs in total, while the third sample corresponds to about 1000 GRBs in total.

2.4 Estimating L_{iso} and the χ^2 test.

For the remaining GRBs that were not used in the calibration procedure, the calibrated relations will be used to find L_{iso} from the values of τ and V . Thus we obtain two estimates:

$$\log L_V = \log B_v + \beta_v \log V, \quad (10)$$

$$\log L_\tau = \log B_\tau + \beta_\tau \log \tau_{lag}. \quad (11)$$

These two estimates are combined as weighted averages to produce one estimate of L_{iso} ,

$$\log L_{iso} = \frac{1}{2} \left(\frac{1}{\sigma_{\log L_V}} \log L_V + \frac{1}{\sigma_{\log L_\tau}} \log L_\tau \right). \quad (12)$$

The next step consists in defining the χ^2 function,

$$\chi^2(\mathbf{p}) = \sum_i^{N_{GRB}} \left(\frac{m_i - M_i - 25 - 5 \log d_L(z_i, \mathbf{p})}{\sigma_\mu} \right)^2, \quad (13)$$

where m_i is the observed magnitude, M_i is the absolute magnitude estimated from Eqs. (10) and (11), and $d_L(z_i, \mathbf{p})$ is the standard luminosity distance as function of redshift z and the cosmological parameters \mathbf{p} . The denominator σ_μ is the uncertainty in the determination of the distance modulus, $m_i - M_i$. This uncertainty was calculated using Gaussian error propagation, and assuming that there were no correlation terms to be taken into account. The values of σ_μ we have found are shown in Table 2. We have to minimize this function and draw the χ^2 contours in order to find the confidence regions.

In here we follow the method developed for the study of SNe Ia (Goliath et al. 2001; Weller & Albrecht 2002; Di Pietro & Claeskens 2003; Silva & Bertolami 2003). We use the log-likelihood function χ^2 to build confidence regions in the parameter space. In order to perform this one chooses a fiducial model, denoted by the parameter vector \mathbf{p}_{fid} , and then the log-likelihood functions χ^2 are calculated based on hypothetical magnitude measurements at the various redshifts. The χ^2 function is then given by

$$\chi^2(\mathbf{p}) = \sum_i^{N_{GRB}} \left(\frac{5 \log d_L(z_i, \mathbf{p}_{fid}) - 5 \log d_L(z_i, \mathbf{p})}{\sigma_\mu} \right)^2. \quad (14)$$

Of course, there is no need to minimize the χ^2 function since its minimum will correspond to $\mathbf{p} = \mathbf{p}_{fid}$, thus we only need to find the χ^2 contours corresponding to the desired confidence level.

2.5 The models.

The GCG model smoothly interpolates between a dark matter dominated time in the past, to an accelerated de Sitter phase in the future. Thus, this is a setting that on large scales agrees with the observed expansion history of the Universe (Kamenshchik et al. 2001; Bento et al. 2002b). The GCG density may be written as a function of redshift as

$$\rho_{ch}(z) = \rho_{ch,0} \left[A_s + (1 - A_s)(1 + z)^{3(1+\alpha)} \right]^{1/(1+\alpha)} \quad (15)$$

where $\rho_{ch,0}$ is the present day density of the GCG, and

$$A_s \equiv A \rho_{ch,0}^{-(1+\alpha)}; \quad (A + B)^{1/(1+\alpha)} = \rho_{ch,0}, \quad (16)$$

where B is the integration constant that appears in Eq. (2). For $z \gg 0$ we have a matter dominated Universe,

$$\rho_{ch}(z \gg 0) = (1 - A_s)^{1/(1+\alpha)} (1 + z)^3, \quad (17)$$

while in the far future, $z = -1$ the GCG behaves as a vacuum dominated Universe.

The GCG unifies dark matter and dark energy, but does not take into account the presence of baryons and radiation. The baryonic component has to be considered when studying the implications of the GCG model with regards to observational tests, but for geometric tests, such as the magnitude-redshift relation we consider here, the effect of these components is negligible. Therefore, throughout the paper we disregard the presence of baryons and radiation. This does not affect any of our conclusions.

For the purpose of comparison we choose the so-called XCDM model, which consists of two components, cold dark matter and some form of dark energy which has a constant negative equation of state, $w = p/\rho$. We shall use this parameterization to

test GRBs as a probe of an unspecified dark energy component. Although this parameterization is not suitable for general dark energy models, since in most cases the equation of state changes with time, it is adequate to test the cosmological constant model, $w = -1$, against other models. If one finds that $w = -1$ is disfavoured by the data, then there is a strong indication that the dark energy component is more complex than expected.

For many years cosmologists were mainly concerned with models to which $-1 \leq w < -2/3$, however, more recently mounting evidence that $w < -1$, the so-called phantom dark energy models (Caldwell 2002; Carroll, Hoffman & Trodden 2003), is being encountered. In many models there are several theoretical reasons not to consider $w < -1$, most notably that this would lead to a breakdown of the weak, the dominant and the strong energy conditions ($\rho \geq 0$ and $\rho + p \geq 0$, $\rho \geq |p|$, and $\rho + 3p \geq 0$, respectively). The weak and strong energy conditions are ones to hold in proving well known singularity theorems, while the dominant energy condition guarantees the stability of a component, such that there is no creation of energy-moment from nothing (Hawking & Ellis 1973).

Another feature of some phantom models is that they exhibit a future blow up of the scale factor in a finite time, often referred to as the ‘Big-Rip’. Since such a Universe has a finite lifetime, it has been argued that these phantom models solve the coincidence problem, that is, they explain why dark matter and dark energy densities are of the same order at the present time. For a Λ CDM Universe, a long matter dominated period is followed by a rather quick transition to a phase such as the one the Universe is now, where matter and dark energy have approximate densities. This phase is then followed by an eternal vacuum dominated exponential expansion. Within this framework, the probability of finding ourselves in this intermediate and temporary epoch is very small. For phantom models on the other hand, the accelerated expansion is not eternal. Since the Universe has a finite lifetime, the probability of living in the epoch of matter-energy approximate equality is larger than that of Λ CDM models, thus, the cosmic coincidence is not as unlikely as for Λ CDM models. However, these models fail to explain why the dark energy component did not start to dominate the evolution at an earlier time, namely, why dark energy started dominating the cosmic evolution only after the large scale structure had time to evolve deep into the non-linear regime, even though in the context of the CGC this is exactly what is found (Bento et al. 2004).

Furthermore, besides these theoretical features, the latest SNe Ia data does seem to favour a phantom energy component. Thus, in what follows, we shall consider a phantom model for comparison with the GCG model. Moreover, as shown in Bertolami et al. (2004) and Bento et al. (2005), for $z < 2$, the GCG model is degenerate with phantom models with suitable parameters.

As mentioned, we consider two different cosmological models. The flat GCG model, which unifies dark energy and dark matter into a single component, and the XCDM, which parameterizes dark energy in terms of a constant equation of state, $w = p/\rho$. We consider that the Universe is flat in both models. The GCG model is then described by the exponent α , and the quantity A_s , while the XCDM is described by the parameters w and Ω_m , the non-relativistic dark matter density relative to the critical one. We considered two fiducial models. Model I assumes that the Universe is described by a GCG model with $1 - A_s = 0.3$ and $\alpha = 1$. Model II assumes the corresponding degenerate Universe, described by a phantom XCDM model, with $w = -1.4$ and $\Omega_m = 0.45$.

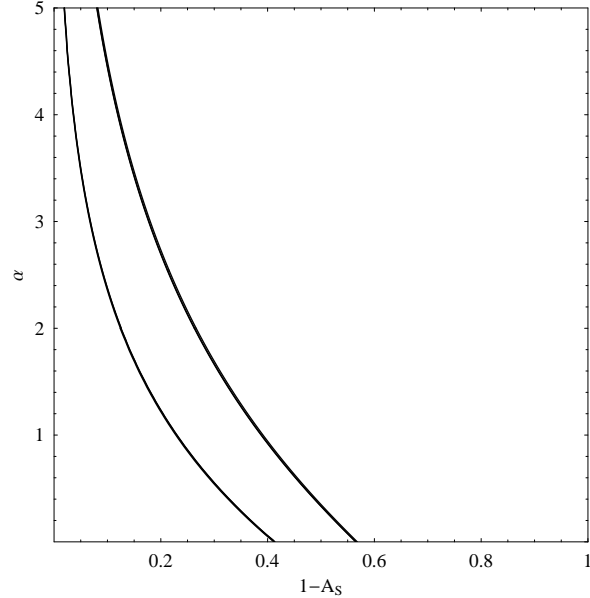


Figure 2. Effects of the improvement in calibration of GRBs for CGC models. The three sets of curves are indistinguishable.

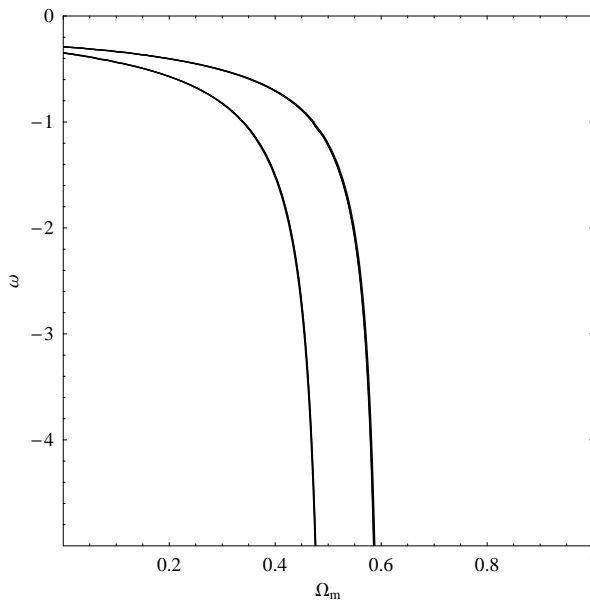


Figure 3. Effects of the improvement in calibration of GRBs for XCDM models. The three sets of curves are indistinguishable.

3 RESULTS.

We first examined the effect that an improvement in the calibration might have in constraining the models. To that end we consider that the high-redshift GRBs sample is comprised by 90 GRBs with redshifts $z > 1.5$, and use the values shown in Table 2 to calculate the uncertainty in the determination of L_{iso} . The effect that an improvement in calibration has in the quality of the cosmological tests is shown in Figures 2 and 3.

We then tested the effect of an increase in the number of high-redshift GRBs in the test. We assume for the purpose of calibration

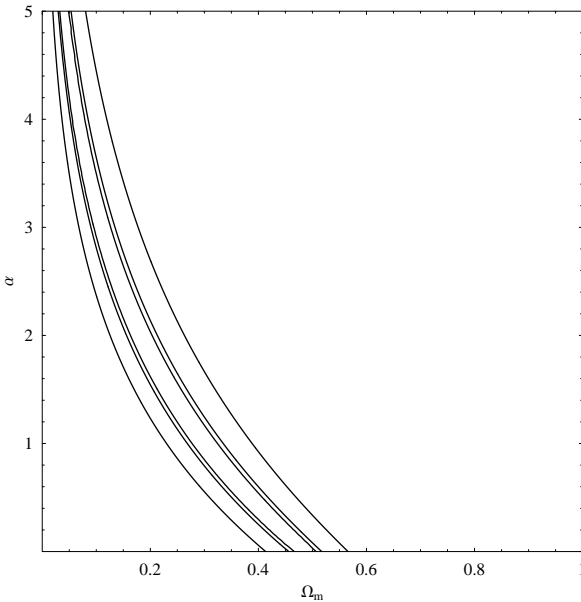


Figure 4. Effects of the increase in the number of GRBs for CGC models. The curves correspond, from the outer to the inner ones, to 90, 500 and 1000 high-redshift GRBs

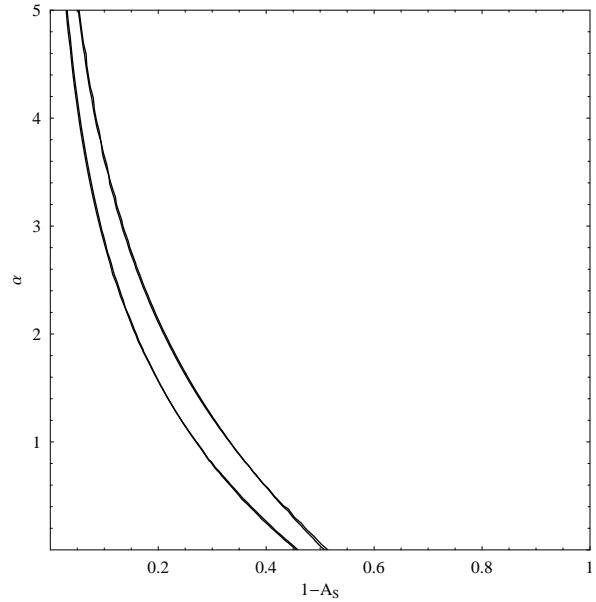


Figure 6. Effect of adding 100 low-redshift GRBs to a sample of 500 high-redshift GRBs for CGC models. Both sets of curves are indistinguishable.

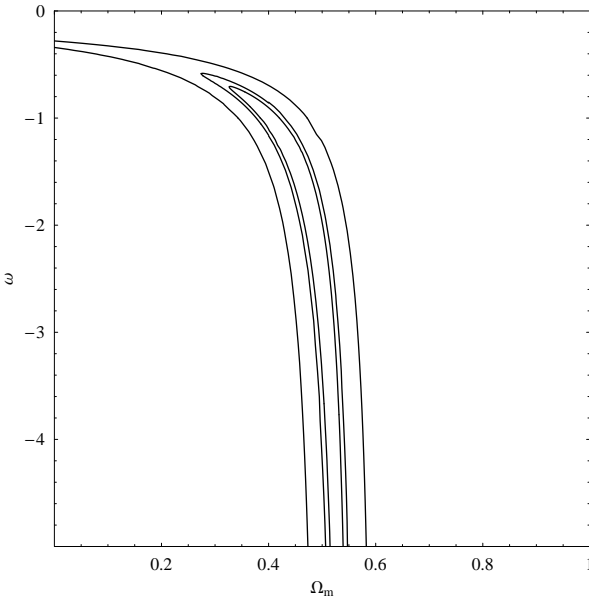


Figure 5. Effects of the increase in the number of GRBs for XCDM models. The curves correspond, from the outer to the inner curves, to 90, 500 and 1000 high-redshift GRBs.

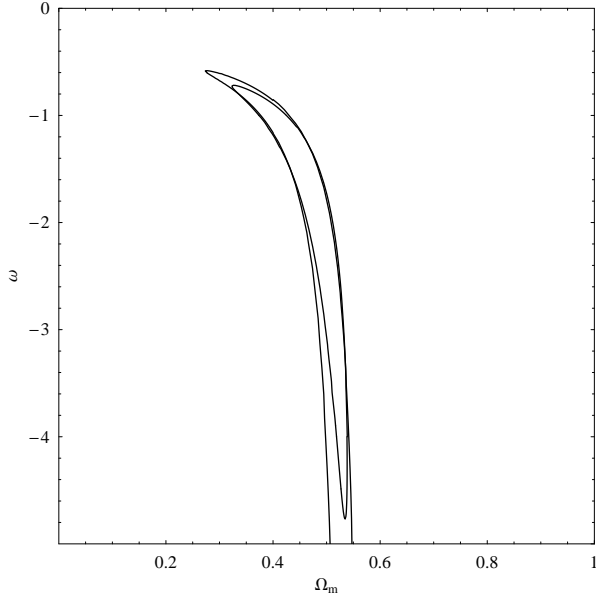


Figure 7. Effect of adding 100 low-redshift GRBs to a sample of 500 high-redshift GRBs for XCDM models. The outer curve corresponds to 500 high-redshift GRBs, while the inner one corresponds to the 100+500 GRB case.

that 100 low-redshift GRBs are known, and use the corresponding calibration precision shown in Table 2. We next considered larger samples of GRBs. Samples with 90, 500 and 1000 high-redshift GRBs are examined, and the respective confidence regions are exhibited. These results are shown in Figures 4 and 5

Finally we study the effect of the distribution of GRBs in redshift space. In order to perform this analysis we added 100 GRBs with $z < 1.5$ to a sample of 400 high-redshift GRBs, and found the

corresponding confidence regions. The results are shown in Figures 6 and 7.

The first conclusion we can draw is that GRBs are not quite suitable as stand-alone probes of dark energy. This is seen from the lack of impact that an increase in the redshift range has on the results in terms of precision and discriminating power.

The main source of uncertainty comes from the intrinsic statistical scatter of the GRB population. As may be seen from Figures 2 and 3, calibrating the (τ, L_{iso}) and (V, L_{iso}) relations with more than about 30 low-redshift GRBs does not substantially affect the

results, however an increase in the size of the higher redshift GRB population will improve the quality of the constraints that can be imposed. This can be seen in Figures 4 and 5. Using more precise luminosity estimators, such as the one we will use in the following section, might improve the outcome, even though better results can be achieved by probing a greater sample of $z < 1.5$ redshift sources. This is evident for $XCDM$ models, as shown in Figure 7. Adding more 100 GRBs with $z < 1.5$ to a sample of 400 high-redshift GRBs is more effective than adding more 500 GRBs with $z > 1.5$.

Regarding the results for each model, the first conclusion is that the $XCDM$ model is better constrained than the CGC model. It can be seen that, no constraint in the α parameter for the CGC model can be imposed, even though an upper limit for A_s can be obtained.

As for $XCDM$ models, we point out that there is some potential to probe Ω_m , but the prospect of using this test to probe the nature of dark energy is very limited. A upper value for w can be obtained, however no lower limit. It should be noted that other tests such as SNe Ia are capable of imposing tighter constraints on Ω_m than the ones we find.

4 THE GHIRLANDA RELATION.

4.1 Description.

The (τ, L_{iso}) and (V, L_{iso}) relations are notoriously affected by the large intrinsic scatter of the data set, which greatly hinders their use as precision cosmological probes. Quite recently, Ghirlanda et al. (2004a) have found a surprisingly tight correlation between the peak energy of the γ -ray spectrum, E_{peak} (in the $\nu - \nu F_\nu$ plot), and the collimation corrected energy emitted in γ -rays, E_γ , for long GRBs. This collimation corrected energy measures the energy release by the GRB taking into account that the energy is beamed into a jet with aperture angle θ .

Let us denote by E_{iso} the isotropically equivalent energy, inferred from the isotropic GRB emission. This source frame “bolometric” isotropic energy is found integrating the best fit time-integrated spectrum $N(E)$ [photons $\text{cm}^{-2} \text{keV}^{-1}$] over the energy range 1 keV - 10 MeV,

$$E_{iso} = \frac{4\pi d_L^2(z)}{1+z} S_\gamma k \text{ erg} , \quad (18)$$

where $d_L(z)$ is the GRB luminosity distance, k refers to the k-correction (Bloom, Frail & Sari 2001) and S_γ is the fluence,

$$S_\gamma = \int_1^{10^4} EN(E)dE , \quad (19)$$

where E is in keV.

If the γ -ray emission is collimated into a jet with aperture θ , then the true energy emitted is $E_\gamma = E_{iso}(1 - \cos \theta)$. Thus, to convert E_{iso} into E_γ and vice-versa, one needs to know the angle θ . Under the simplifying assumption of a constant circum-burst density medium of number density n , a fireball emitting a fraction η_γ of its kinetic energy in the prompts γ -ray phase would show a break in its afterglow light curve when its bulk Lorentz factor Γ becomes of the order of $\Gamma \simeq 1/\theta$, with θ given by (Sari 1999):

$$\theta = 0.161 \left(\frac{t_{jet}}{1+z} \right)^{3/8} \left(\frac{n\eta_\gamma}{E_{iso,52}} \right)^{1/8} \quad (20)$$

where t_{jet} is the break time in days, and $E_{iso,52} = E_{iso}/10^{52}$.

	Error	Contribution to $(\frac{\sigma_{d_L}}{d_L})^2$	Percentage of $(\frac{\sigma_{d_L}}{d_L})^2$
$\left(\frac{\sigma_{S_\gamma}}{S_\gamma} \right)^2$	10%	0.0027	5%
$\left(\frac{\sigma_k}{k} \right)^2$	5%	0.0006	1%
$\left(\frac{\sigma_C}{C} \right)^2$	8%	0.0027	5%
$\left(\frac{\sigma_a}{a} \right)^2$	5%	0.0025	5%
$\left(\frac{\sigma_{E_p}}{E_p} \right)^2$	17%	0.0259	52%
$\left(\frac{\sigma_n}{n} \right)^2$	50%	0.0069	14%
$\left(\frac{\sigma_{t_{jet}}}{t_{jet}} \right)^2$	20%	0.0081	16%

Table 3. Error budget for the Ghirlanda test. The uncertainty in the circum-burst density is assumed to be 50%, while the other values are taken from Xu (2005).

The Ghirlanda relation (Ghirlanda et al. 2004a; Xu 2005) is then expressed as

$$\frac{E_\gamma}{10^{50} \text{erg}} = C \left(\frac{E_p}{100 \text{ keV}} \right)^a \quad (21)$$

where a and C are dimensionless parameters.

Using this result, together with Eqs. (18), (20) and the definition of E_γ , one obtains an equation for $d_L(z)$,

$$C \left(\frac{E_p}{100 \text{ keV}} \right)^a = (1 - \cos \theta) \left(\frac{E_{iso}}{10^{50}} \right) . \quad (22)$$

Note that both E_{iso} and θ depend on $d_L(x)$, as may be seen from their definitions. Solving this equation for $d_L(z)$ we find an estimate of the luminosity distance at redshift z in terms of the observables E_p , t_{jet} , n , and fluence S_γ .

The error budget for d_L is then found to be (Xu 2005)

$$\begin{aligned} \left(\frac{\sigma_{d_L}}{d_L} \right)^2 &= \frac{1}{4} \left[\left(\frac{\sigma_{S_\gamma}}{S_\gamma} \right)^2 + \left(\frac{\sigma_k}{k} \right)^2 \right] + \frac{1}{4} \frac{1}{(1 - \sqrt{C_\theta})^2} \times \\ &\quad \left[\left(\frac{\sigma_C}{C} \right)^2 + \left(a \frac{\sigma_{E_p}^{obs}}{E_p^{obs}} \right)^2 + \left(a \frac{\sigma_a}{a} \ln \frac{E_p}{100} \right)^2 \right] + \\ &\quad \left[\left(\frac{3\sigma_{t_j}}{t_j} \right)^2 + \left(\frac{\sigma_{n_0}}{n_0} \right)^2 + \left(\frac{\sigma_{\eta_\gamma}}{\eta_\gamma(1 - \eta_\gamma)} \right)^2 \right] \times \\ &\quad \frac{1}{4} \frac{C_\theta}{(1 - \sqrt{C_\theta})^2} , \end{aligned} \quad (23)$$

where $C_\theta^2 = \theta \sin \theta / (8 - 8 \cos \theta)$.

The distance modulus is given by $\mu_{obs} = 5 \log d_L/10\text{pc}$, thus its error is $\sigma_\mu = 5/\ln 5(\sigma_{dL}/d_L)$. We use the error estimates from (Xu 2005), which are consistent with what is found in the literature (Ghirlanda et al. 2004a; Ghirlanda et al. 2004b; Friedman & Bloom 2005; Ghisellini et al. 2005; Xu, Dai & Liang 2005; Mörtsel & Sollerman 2005).

These values yield an uncertainty in μ_{obs} of order $\sigma_\mu \simeq 0.5$, which is just slightly smaller than the error bars from using both the (L_{iso}, V) and (L_{iso}, τ_L) relations. As may be observed in Table 3, the smaller intrinsic scatter of the Ghirlanda relation is balanced by its dependence on poorly constrained quantities. Improving the calibration will not solve the problem, since the main sources of uncertainty are due to the determination of the peak energy E_p , the jet break time t_{jet} and the value of the circum-burst density n .

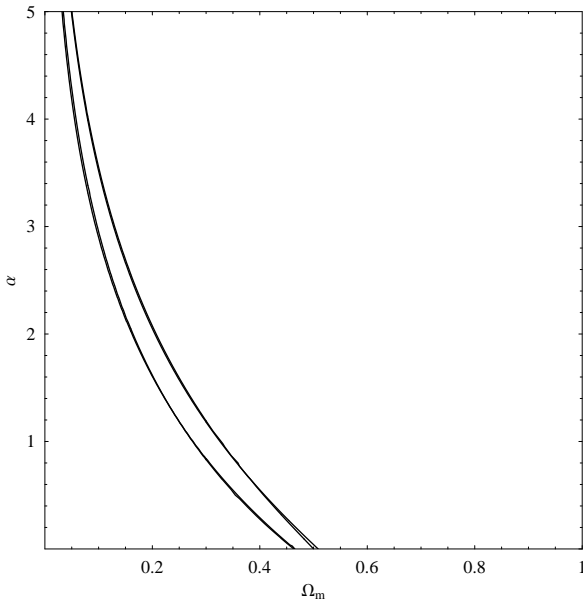


Figure 8. Same as Figure 6, but using the Ghirlanda relation.

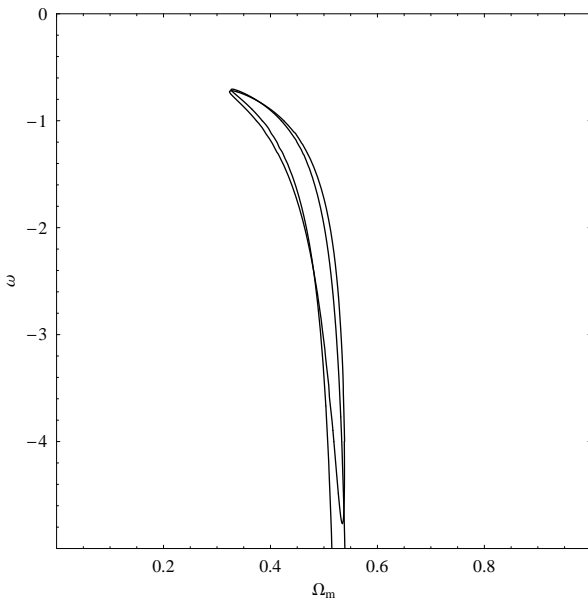


Figure 9. Same as Figure 7, but using the Ghirlanda relation.

4.2 Results.

In Figures 8 and 9 we see the improvements that can be obtained by the use of the Ghirlanda relation. We have assumed two redshift distributions; one made up of 500 GRBs with $z > 1.5$, and the other made up of 100 GRBs with $z < 1.5$ plus 400 GRBs with $z > 1.5$. We find that the conclusions one can draw remain essentially unchanged. Moreover, we see that the high-redshifts of GRBs are not quite suitable to adequately study the GCG model, while it allows for the XCDM model to place a rather useful limit to the total amount of matter, although not much can be learned with respect to the dark energy equation of state.

5 DEGENERACY BETWEEN MODELS.

The CGC and the phantom XCDM models are degenerate at redshifts $z < 2$, as shown in Bertolami et al. (2004) and Bento et al. (2005). Consider the Taylor expansion of the luminosity distance as

$$d_L = \frac{c}{H_0} \left\{ z + \frac{1}{2}(1 - q_0)z^2 - \frac{1}{6}(1 - q_0 - 3q_0^2 + j_0)z^3 - \left[1 + \frac{3}{2}q_0(1 + q_0) + \frac{5}{8}q_0^3 - \frac{1}{2}j_0 - \frac{5}{12}q_0j_0 - \frac{k_0}{24} \right] z^4 + O(z^5) \right\}, \quad (24)$$

where q_0 is the deceleration parameter, related to the second derivative of the expansion factor, j_0 is the so-called ‘‘jerk’’ or statefinder parameter (Alam et al. 2003; Sahni et al. 2003), related to the third derivative of the expansion factor, and k_0 is the so-called ‘‘kern’’ parameter, which is related to the fourth derivative of the expansion parameter (Visser 2004; Dabrowski & Stachowiak 2004), all evaluated at present. These quantities are defined as

$$q(t) = -\frac{1}{a} \frac{d^2 a}{dt^2} \left[\frac{1}{a} \frac{da}{dt} \right]^{-2}; \quad (25)$$

$$j(t) = +\frac{1}{a} \frac{d^3 a}{dt^3} \left[\frac{1}{a} \frac{da}{dt} \right]^{-3}; \quad (26)$$

$$k(t) = +\frac{1}{a} \frac{d^4 a}{dt^4} \left[\frac{1}{a} \frac{da}{dt} \right]^{-4}; \quad (27)$$

and are related to each other through the relations

$$q(z) = \frac{3}{2} \left(\frac{p(z)}{\rho(z)} + 1 \right) - 1; \quad (28)$$

$$j(z) = q(z) + 2q^2(z) + \frac{dq}{dz}(z); \quad (29)$$

$$k(z) = \frac{dq}{dz}(z) - 2j(z) - 3j(z)q(z). \quad (30)$$

where $\rho(z)$ and $p(z)$ refer to the total density and pressure of the Universe, respectively. With these expressions one can write the present day values of the parameters as a function of the cosmological parameters of the model under examination.

For the $XCDM$ model, we have

$$q_0^{XCDM} = \frac{3}{2} [1 + w(1 - \Omega_m - 1)] - 1, \quad (31)$$

$$\frac{dq}{dz} \Big|_0^{XCDM} = \frac{9}{2} w^2 (1 - \Omega_m) \Omega_m, \quad (32)$$

$$\frac{dj}{dz} \Big|_0^{XCDM} = -\frac{9}{2} w^2 (2 - 3w) (\Omega_m - 1) \Omega_m, \quad (33)$$

while for the GCG model we find

$$q_0^{GCG} = \frac{3}{2} (1 - A_s) - 1 \quad (34)$$

$$\frac{dq}{dz} \Big|_0^{GCG} = \frac{9}{2} A_s (1 - A_s) (1 + \alpha), \quad (35)$$

$$\frac{dj}{dz} \Big|_0^{GCG} = 1 + \frac{9}{2} \alpha (1 - A_s) A_s. \quad (36)$$

For the redshift range probed by SNe Ia one may neglect terms beyond the cubic power in redshift in Eq. (24). SNe Ia data indicate that these models have the same deceleration and jerk (Bertolami et al. 2004; Bento et al. 2005), that is, they are degenerate for the considered redshift range. Thus, imposing this equality one finds the relationship between parameters

$$w = \alpha(A_s - 1) - 1, \quad (37)$$

$$\Omega_m = \frac{(1 + \alpha)(1 - A_s)}{1 + \alpha(1 - A_s)}. \quad (38)$$

This degeneracy holds for SNe Ia, for the maximum probed redshift of about $z \approx 2$. As the redshift range allowed by GRBs is greater, one hopes to test higher order terms in Eq. (24). At next order, the degeneracy is broken by the jerk parameter, that is, even if $q_0^{GCG} = q_0^{XCDM}$, $j_0^{GCG} = j_0^{XCDM}$, one finds that $k_0^{GCG} \neq k_0^{XCDM}$. For instance, if one considers $\alpha = 1$ and $A_s = 0.7$, then $k_0^{GCG} = -0.3$, while for the corresponding $XCDM$ model (with $w = -1.3$ and $\Omega_m = 0.46$), the jerk is $k_0^{XCDM} = -4.27$.

This procedure can be viewed as a consistency test. Indeed, consider the GCG model. Once the deceleration, the jerk and the jerk of the Universe are measured, one can extract the values of α and A_s . These values yield a value for the jerk, call it k_0^t , which can be compared to the measured value of the jerk, k_0^m . Whether both values are close or not, one may reach a conclusion regarding the suitability of the model. The same reasoning can be applied to the $XCDM$ model. This is, of course, a simplification, since one has to consider the accuracy of measurements and the statistical significance of each of the parameters in Eq. (24), as well as to consider correlations between them.

6 DISCUSSION AND CONCLUSIONS.

We have verified that the medium and high redshift of GRBs do not impose too strong constraints on the GCG model. At such high redshifts, the expansion factor for the GCG becomes

$$H_{ch}(z \gg 0) = \Omega_{ch}(1 - A_s)^{1/(1+\alpha)}(1 + z)^3 \quad (39)$$

where Ω_{ch} is the GCG density relative to the critical one. Since we are considering a flat Universe made up mostly by the GCG, $\Omega_{ch} = 1$. Thus, the luminosity distance at such high redshifts depends essentially on $(1 - A_s)^{1/(1+\alpha)}$. It is found that the confidence regions for the GCG model approximately follow the line $(1 - A_s)^{1/(1+\alpha)} = \text{const}$. Hence, since A_s and α are strongly correlated by this expression, neither one is constrained.

As for the $XCDM$ model, a high-redshift population of GRBs is suitable to constrain the total amount of matter, Ω_m , but are poor probes of the dark energy equation of state. This does not mean that GRBs have no use for the study of dark energy, or that expanding the Hubble diagram is meaningless. It is a common trend in the recent literature to argue that a precise prior estimate of Ω_m enhances the ability of SNe Ia to constrain the dark energy equation of state (Goliath et al. 2001; Weller & Albrecht 2002; Di Pietro & Claeskens 2003). This is also true for GRBs. A high-redshift sample will constrain Ω_m , while a low-redshift sample will place constraints on the equation of state. A low-redshift sample alone will fail to constrain the equation of state since it will be hindered by large uncertainties in Ω_m . This is somewhat similar to what happens in SNe Ia tests. A low-redshift sample will constrain the nuisance parameter \mathcal{M} , while the high-redshift sample constrains the cosmological parameters (Padmanabhan & Choudhury 2003; Choudhury & Padmanabhan 2005).

Our study also reveals that the effectiveness of the GRB test depends on the model under examination. GRBs allow imposing some constraints on the $XCDM$ model, but very little can be extracted for the GCG model. This may be explained by two factors. The first was explained above, and is related to the fact that the

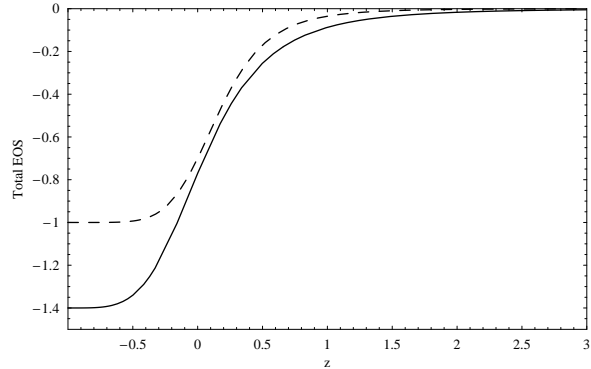


Figure 10. Total equation of state of the Universe as a function of redshift. The value $z = -1$ corresponds to the very far future. The dashed line represents our GCG fiducial model, while the solid line corresponds to the $XCDM$ phantom model.

region probed by GRBs depends on an unique function of both parameters. The second is related to how late the Universe stops being matter dominated. As shown in Figure 10, the GCG model stays in the matter dominated phase for a longer time, thus the period of time during which the dark energy behaviour affects the cosmic expansion is slightly larger for the $XCDM$ model. Since GRBs essentially probe larger redshifts, models in which the transition between the matter dominated and accelerated expansion is shorter cannot be well constrained by this test. By the same reasoning, GRBs might be actually useful in testing models where the transition between matter dominated expansion and dark energy driven acceleration started at larger redshifts.

Thus, we find that despite all intrinsic limitations, larger samples of GRBs can potentially determine the total amount of matter in a $XCDM$ model. This independent determination of Ω_m will be useful in SNe Ia studies of the dark energy equation of state.

Furthermore, GRBs may also be used to break the degeneracy between models, since at high-redshifts the effect of higher order terms in the Taylor expansion of $d_L(z)$ must be taken into account.

REFERENCES

Alam U., Sahni V., Saini T.D., Starobinsky A.A., 2003, MNRAS 344, 1057
 Albrecht A., Skordis C., 2000, Phys. Rev. Lett., 84, 2076
 Alcaniz J.S., Jain D., Dev A., 2003, Phys. Rev. D, 67, 043514.
 Amendola L., 1999, Phys. Rev. D, 60, 043501
 Amendola L., Finelli F., Burigana C., Caturan D., 2003, JCAP, 0307, 005
 Band D., et al., 1993, ApJ 413, 281
 Barris B.J., et al., 2004, ApJ, 602, 571
 Bento M.C., Bertolami O., 1999, Gen. Relat. & Grav., 31, 1461
 Bento M.C., Bertolami O., Santos N.C., 2002, Phys. Rev. D, 65, 067301
 Bento M.C., Bertolami O., Santos N.M.C., Sen A.A., 2005, Phys. Rev. D, 71, 063501
 Bento M.C., Bertolami O., Sen A.A., 2002b, Phys. Rev. D, 66, 043507
 Bento M.C., Bertolami O., Sen A.A., 2003a, Phys. Lett. B, 575, 172
 Bento M.C., Bertolami O., Sen A.A., 2003b, Phys. Rev. D, 67, 063003
 Bento M.C., Bertolami O., Sen A.A., 2003c, Gen. Relat. and Gravitation, 35, 2063
 Bento M.C., Bertolami O., Sen A.A., 2004, Phys. Rev. D, 70, 083519
 Bento M.C., Bertolami O., Silva P.T., 2001, Phys. Lett. B, 498, 62
 Bertolami O., 1986a, Il. Nuovo Cimento, 93B, 36
 Bertolami O., 1986b, Fortschr. Physik, 34, 829
 Bertolami O., 2004, preprint (astro-ph/0403310)
 Bertolami O., 2005, preprint (astro-ph/0504275)

Bertolami O., Martins P.J., 2000, Phys. Rev. D, 61, 064007
 Bertolami O., Sen A.A., Sen S., Silva P.T., 2004, MNRAS 353, 329
 Bilic N., Tupper G.B., Viollier R. D., 2002, Phys. Lett. B, 535, 17
 Bloom J.S., Frail D.A., Sari R., 2001, Astron. J. 121, 2879
 Bordemann M., Hoppe J., 1993, Phys. Lett. B, 317, 315
 Bronstein M., 1933, Phys. Zeit. Sowjet Union, 3, 73
 Caldwell R.R., 2002, Phys. Lett. B, 545, 23
 Caldwell R.R., Dave R., Steinhardt P.J., 1998 Phys. Rev. Lett., 80, 1582
 Carroll S. M., Hoffman M., Trodden M., 2003, Phys. Rev. D, 68, 023509
 Caturan D., Finelli F., 2003, Phys. Rev. D, 68, 103501
 Choudhury T.R., Padmanabhan T., 2005, A&A 429, 807
 Binétruy P., 1999, Phys. Rev. D, 60, 063502
 Chiba T., 1999, Phys. Rev. D, 60, 083508
 Dabrowski M.P., Stachowiak T., 2004, preprint (astro-ph/0411199)
 Dev A., Alcaniz J.S., Jain D., 2003, Phys. Rev. D, 67, 023515
 Dev A., Jain D., Alcaniz J.S., 2004, A&A, 417, 847
 Fabris J.C., Gonçalves S.B.V., de Souza P.E., 2002a, preprint (astro-ph/0207430)
 Fabris J.C., Gonçalves S.B.V., de Souza P.E., 2002b, Gen. Relat. and Gravitation, 34, 53
 Ferreira P.G., Joyce M., 1998, Phys. Rev. D, 58, 023503
 Friedman A.S., Bloom J.S., 2005, preprint (astro-ph/0502559)
 Frolov A., Kofman L., Starobinsky A., 2002, Phys. Lett. B, 545, 8
 Fujii Y., 2000, Phys. Rev. D, 61, 023504
 Ghirlanda G., Ghisellini G., Lazzati D., 2004a, ApJ, 616, 331
 Ghirlanda G., Ghisellini G., Lazzati D., Firmani C., 2004b, ApJ, 613, L13
 Ghisellini G., Ghirlanda G., Firmani C., Lazzati D., Avila-Reese V., 2005, preprint (astro-ph/0504306)
 Goliath M., Amanullah R., Astier P., Goobar A., Pain R., 2001 A&A 380, 6
 Gorini V., Kamenshchik A., Moschella U., 2003, Phys. Rev. D, 67, 063509
 Hawking S.W., Ellis G.F.R., 1973, The Large Scale Structure Of Space-Time, Cambridge University Press
 Huterer D., Turner M.S., 2000, Phys. Rev. D, 64, 123527
 Jackiw R., Polychronakos A.P., 2000, Phys. Rev. D, 62, 085019
 Kamenshchik A., Moschella U., Pasquier V., 2000, Phys. Lett. B, 487, 7
 Kamenshchik A., Moschella U., Pasquier V., 2001, Phys. Lett. B, 511, 265
 Kim J.E., 1999, JHEP, 9905, 022
 Lamb D.Q., Reichart D.E., 2000, ApJ 536, 1
 Makler M., de Oliveira S.Q., Waga I., 2003, Phys. Lett. B, 555, 1
 Mörtzell E., Sollerman J., 2005, preprint (astro-ph/0504245)
 Norris J.P., Marani G.F., Bonnell J.T., 2000, ApJ 534, 248
 Ozer M., Taha M.O., 1987, Nucl. Phys. B, 287, 776
 Padmanabhan T., Choudhury T.R., 2003, MNRAS 344, 823
 Di Pietro E., Claeskens J.F., 2003, MNRAS 341, 1299
 Porciani C., Madau P., 2000, ApJ, 548, 522
 Ratra B., Peebles P.J.E., 1988a, Phys. Rev. D, 37, 3406
 Ratra B., Peebles P.J.E., 1988b, ApJ, L325, 117
 Reichart D.E., Lamb D.Q., Fenimore E.E., Ramirez-Ruiz E., Cline T.L., Hurley K., 2001, ApJ 551, 57
 Riess A.G., et al. [Supernova Search Team Collaboration], ApJ, 607, 665
 Sandvik H., Tegmark M., Zaldarriaga M., Waga I., 2004, Phys. Rev., D, 69, 123524
 Sahni V., Saini T.D., Starobinsky A.A., Alam U., 2003, JETP Lett. 77, 201
 Sari R., 1999, ApJ 524, L43
 Sen A.A., Sen S., 2001, Mod. Phys. Lett., A16, 1303
 Sen A.A., Sen S., Sethi S., 2001, Phys. Rev. D, 63, 107501
 Silva P.T., Bertolami O., 2003, ApJ 599, 829
 Schaefer B.E., 2000, ApJ, 583, L67
 Tonry J.L., et al., 2003, ApJ, 594, 1
 Takahashi K., Masamune O., Kei K., Hiroshi O., 2003, preprint (astro-ph/0305260)
 Uzan J.P., 1999, Phys. Rev. D, 59, 123510
 Visser M., 2004, Class. Quant. Grav. 21, 2603
 Weller J., Albrecht A., 2002, Phys. Rev. D, 65, 103512
 Wetterich C., 1988, Nucl. Phys. B, 302, 668
 Xu D., 2005, ApJ, submitted (astro-ph/0504052)
 Xu D., Dai Z.G., Liang E.W., 2005, preprint (astro-ph/0501458)
 Zlatev I., Wang L., Steinhardt P.J., 1999, Phys. Rev. Lett., 82, 986